Annealing Effects on Zn(Co)O: From Para- to Ferromagnetic Behavior

R. Boubekri,[†] Z. Beji,[†] K. Elkabous,[†] F. Herbst,[†] G. Viau,[†] S. Ammar,*[,†] F. Fiévet,[†] H. J. von Bardeleben,[‡] and A. Mauger[§]

ITODYS, UMR-CNRS 7086, Université Paris 7, 2 place Jussieu, 75251 Paris, France, Institut des NanoSciences de Paris, UMR-CNRS 7588, and Institut de Minéralogie et de Physique des Milieux Condensés, Université Paris 6, 140 rue de Lourmel, 75015 Paris, France

Received September 25, 2008. Revised Manuscript Received December 12, 2008

$Zn_{1-x}Co_xO$ nanocrystals were produced by forced hydrolysis in diethyleneglycol. The as-produced crystals are paramagnetic. However, heating at 400 °C under a nitrogen atmosphere for 1 h induces ferromagnetism at room temperature, characterized by coercive field (0.38 kOe) and magnetization at 10 kOe (0.10 μ_B/Co) similar to the values reported recently for nanocrystalline Co:ZnO aggregates. To understand this evolution, we have characterized the samples by chemical and physical analyses including X-ray diffraction (XRD), transmission electron microscopy (TEM), UV−visible−IR absorption spectroscopy, magnetic measurements, and EPR experiments. These analyses show that the Co ions are incorporated into the wurtzite structure, forming a $Zn_{1-x}Co_xO$ solid solution. X-ray diffraction and electron microscopy failed to detect secondary phases, neither before nor after the thermal treatment. However, the shape of the nanoparticles is modified and becomes more spherical upon annealing, which gives evidence of an important diffusion of atomic species. X-band electron paramagnetic resonance (EPR) reveals the presence of magnetic clusters in the annealed samples. Both the magnetic and optical properties show that these are Co clusters that have grown at the expense of the cobalt diluted in the host matrix. The thermal treatment survey performed by thermogravimetric analysis coupled with mass spectrometry and IR spectroscopy gives evidence of desorption of organic species and liberation of oxygen from the surface of the particles. This study then suggests that the origin of the magnetism believed to be intrinsic to the material in many prior works is extrinsic in nature and is due to the diffusion of cobalt and oxygen species at the surface of the particles, where Co forms nanoclusters while most of the oxygen is liberated in the annealing process.

Introduction

Recent progress in the domain of spin electronics, based on the study of the active control and manipulation of charge and spin degrees of freedom of electrons or holes in nanostructures, has led to a revival of a very important class of materials, the diluted magnetic semiconductors (DMS). Among them, ZnO doped with 3d transition metal ions (Mn, Fe, Co, or Ni) has been particularly studied, because it was predicted to exhibit ferromagnetic ordering (FM) at room temperature (RT).[1] In most studies of transition-metal-doped ZnO, no ferromagnetism is observed; however, in some cases, ferromagnetism could be systematically induced by special annealing treatments or particular preparation conditions. For example, polycrystalline $Zn_{1-x}Mn_xO$ powders synthesized by ceramic route exhibit a stable ferromagnetic state at room temperature when they are prepared at 500−700 °C[2] but not when they are prepared at 900 °C.[3] Recent studies on single-phase thin films have shown that n-type single phase $Zn_{1-x}Mn_xO$ thin films are not ferromagnetic and are actually dominated by antiferromagnetic interactions that are even stronger than in the other Mn-doped II−VI DMS.[4] Polycrystalline $Zn_{1-x}Co_xO$ films produced by laser ablation (PLD) were found to be ferromagnetic with a Curie temperature higher than 300 K,[5] whereas similar ones produced by the molecular beam epitaxial (MBE) technique are not.[6]

Ferromagnetic Cu^+-doped $Zn_{0.95}Fe_{0.05}O$[7] and $Zn_{0.98}Co_{0.02}O$[8] powders were synthesized by a ceramic route in an inert atmosphere. Oxygen-deficient ferromagnetic $Zn_{0.75}Co_{0.25}O$ films were also prepared by pulsed laser deposition at low oxygen pressure.[9] Ferromagnetism has also been reported

* Corresponding author. E-mail: ammarmer@univ-paris-diderot.fr.
[†] Université Paris 7.
[‡] Institut des NanoSciences de Paris, UMR-CNRS 7588, Université Paris 6.
[§] Institut de Minéralogie et de Physique des Milieux Condensés, Université Paris 6.

(1) Dietl, T.; Ohno, H.; Matsukura, F.; Cibert, J.; Ferrand, D. *Science* **2000**, *287*, 1019.
(2) Sharma, P.; Gupta, A.; Rao, K. V. O.; Sharma, R.; Ahuja, R.; Osorio, G. J. M.; Johansson, B.; Gehring, G. A. *Nat. Mater.* **2003**, *2*, 673.
(3) Kolesnik, S.; Dabrowski, B. *J. Appl. Phys.* **2004**, *96*, 5379.
(4) (a) Ben Mahmoud, A.; von Bardeleben, H. J.; Cantin, J. L.; Chikoidze, E.; Mauger, A. *J. Appl. Phys.* **2007**, *101*, 013902. (b) Ben Mahmoud, A.; von Bardeleben, H. J.; Cantin, J. L.; Mauger, A.; Chikoidze, E.; Dumont, Y. *Phys. Rev. B* **2006**, *74*, 115203.
(5) Ueda, K.; Tabata, H.; Kawai, T. *Appl. Phys. Lett.* **2001**, *79*, 988.
(6) Jin, Z.; Fukumura, T.; Kawasali, M.; Ando, K.; Saito, H.; Sekiguchi, T.; Yoo, Y. Z.; Murakami, M.; Matsumoto, T.; Koinuma, H. *Appl. Phys. Lett.* **2001**, *78*, 3824.
(7) Todaka, Y.; Nakamura, M.; Hattori, S.; Tsuchiya, K.; Umemoto, M. *Nippon Kinzoku Gakkaishi* **2002**, *66*, 34.
(8) Lin, H. T.; Chin, T. S.; Shih, J. C.; Lin, S. H.; Hong, T. M.; Huang, R. T.; Chen, F. R.; Kai, J. J. *Appl. Phys. Lett.* **2004**, *85*, 621.
(9) Rode, K.; Anane, A.; Mattana, R.; Contour, J. P.; Durand, O.; LeBourgeois, R. *J. Appl. Phys.* **2003**, *93* (10), 7676.

10.1021/cm802605u CCC: $40.75
Published on Web 02/06/2009

in N-doped $Zn_{1-x}Mn_xO$ and interstitial Zn-doped $Zn_{1-x}Co_{0.09}O$ thin films, which were prepared with NO and N_2O sources using a radio frequency plasma route,[10] and by MOCVD with subsequent exposure to zinc vapors at 500 °C,[11] respectively. In all these cases, however, the intrinsic nature of the ferromagnetism has not been established and the origin of the ferromagnetism, when it is observed, is still subject to debate. Clearly, in all these cases, the value of the magnetization demonstrates that only a small fraction of the Co ions contribute to the ferromagnetism. The possibility of an extrinsic ferromagnetism generated by ferromagnetic clusters of an impurity phase is now more and more supported. Indeed, recent extended X-ray absorption fine structure (EXAFS) measurements at the Co K-edge of ferromagnetic $Zn_{1-x}Co_xO$ ($x > 0.12$) thin films, prepared by sol−gel and subsequently annealed at 600 °C under reduced oxygen partial pressure, provided direct evidence for the presence of Co metal clusters.[12] Previous electron paramagnetic resonance spectroscopy (EPR) studies of low doped $Zn_{1-x}Co_xO$ films prepared by PLD had only shown a paramagnetic Curie−Weiss like behavior with the absence of any long-range order.[13]

In this context, we investigated a new synthesis method of $Zn_{1-x}Co_xO$ that would exclude the formation of magnetically active extrinsic phases. We have prepared $Zn_{1-x}Co_xO$ powders by forced hydrolysis of acetate metallic salts in a polyol that has been shown to form ZnO in the wurtzite phase. Hydrolysis in polyol medium is an attractive chimie douce route for producing nanocrystalline $Zn_{1-x}Co_xO$ solid solutions in a large composition range. It is a low-temperature process which allows higher doping levels of magnetic ions in ZnO than conventional synthesis processes; furthermore, it is more efficient than other chimie douce routes (coprecipitation, sol−gel, microemulsion, etc.), as it leads to a higher crystalline quality of the produced nanocrystals.[14]

We have chosen a cobalt doping concentration of $x \approx 0.16$ for two reasons: it is large enough to generate important magnetic interactions between the Co ions in substitution to Zn, and it is still below the solubility limit of Co in ZnO, estimated to $x = 0.20$.[15]

We have equally investigated the effect of a thermal annealing. For this purpose, we have moderately heated the samples under nitrogen atmosphere (at $T = 400$ °C). As we will show below, it is this annealing that introduced a ferromagnetic phase. However, the full analysis of the magnetic properties reported in this work shows that this ferromagnetism is not intrinsic and it cannot be attributed to the generation of donor defects such as oxygen vacancies.[16] Instead, we find that the ferromagnetic component is actually due the formation of Co clusters at the surface, which is accompanied by the departure of surface adsorbed organic species (polyol and/or acetate) and the loss of oxygen.

Our samples have been characterized by X-ray diffraction (XRD), transmission electron microscopy (TEM), SQUID magnetization measurements, and EPR. In particular, the correlation of the EPR and magnetization measurements was found to be decisive to evidence the presence of Co clusters that could not be detected by the other characterization techniques.

Experimental Section

1. Synthesis. Precursor salts, $Zn(CH_3COO)_2 \cdot 2H_2O$ (4.39 g, 0.02 mol) and $Co(CH_3COO)_2.4H_2O$ (1.24 g, 0.005 mol) were added to a given volume (125 mL) of diethyleneglycol. On the basis of previous experiments that evidenced the Co content in the final oxide is always slightly smaller than the nominal composition,[14] we fixed the nominal Co/(Co+Zn) atomic ratio at 0.20 to reach a final one close to 0.16. The mixture was then heated to the boiling point (198 °C) with a heating rate of 6 °C min^{-1}. A wurtzite phase is formed via a chemical process involving the formation of an intermediate purple-colored phase, which corresponds to a Zn−Co hydroxy-acetate layered salt.[17] The mixture was refluxed for 2 h to obtain the final product as a pure solid phase, with a characteristic green color. After being cooled to room temperature, the particles were separated from the supernatant by centrifugation, washed with ethanol, and then dried in air at 50 °C. The powder was then heated under nitrogen for 1 h at 400 °C. In the following sections, the as-produced powder and the 400 °C heat-treated powders are called samples A and B, respectively.

2. Characterization Techniques. The crystal structure of the powders was examined by a Panalytical X'pert Pro diffractometer equipped with a multichannel detector (X'celerator), using the Co K_α radiation ($\lambda = 1.7889$ Å).

Zinc, cobalt, carbon, and hydrogen contents were determined by inductive coupling plasma-atomic emission spectroscopy (ICP) at the Vernaison Analysis Centre of CNRS (France).

The size and shape of the particles were analyzed on a JEOL-100-CX II TEM microscope operating at 100 kV. High-resolution transmission electron microscopy (HRTEM) images were obtained using a Jeol-JEM2010-UHR operating at 200 kV.

UV−visible−NIR diffuse reflectance spectra (DRS) were recorded at room temperature between 190 and 2500 nm on a Varian Cary 5E spectrometer equipped with a double monochromator and an integrating sphere coated with polytetrafluoroethylene (PTFE). PTFE was used as reference.

IR spectra were recorded with a FT-IR Perkin-Elmer 1750 spectrophotometer in the transmittance mode between 4000 and 500 cm^{-1} with a resolution of 4 cm^{-1} and with at least 20 scans. Samples were prepared as KBr pellets. Variable-temperature infrared spectroscopy was performed in the diffuse reflectance mode under static nitrogen gas in a Harrick praying mantis apparatus on pure powder.

Thermogravimetric analysis (TGA) was carried out with a heating rate of 5 °C min^{-1} in an alumina crucible under nitrogen in a Setaram TG92−12 thermal analyzer. Thermal analysis (Setaram balance TG DSC111) coupled with mass spectrometric analysis (Leybold Inficom H 300 CIS spectrometer) was carried out in a platinum crucible under argon with a heating rate of 5 °C min^{-1} up to 600 °C.

(10) Matsui, H.; Saeki, H.; Kawai, T.; Tabata, H.; Mizobuchi, B. *J. Appl. Phys.* **2004**, *95*, 5882.
(11) Schwartz, D. A.; Gamelin, D. R. *Adv. Mater.* **2004**, *16*, 2115.
(12) Park, J. H.; Kim, M. G.; Jang, H. M.; Ryu, S.; Kim, Y. M. *Appl. Phys. Lett.* **2004**, *84*, 1338.
(13) Jedrecy, N.; von Bardeleben, H. J.; Zheng, Y.; Cantin, J. L. *Phys. Rev. B* **2004**, *69*, 041308(R) .
(14) Poul, L.; Ammar, S.; Jouini, N.; Fiévet, F.; Villain, F. *Solid State Sci.* **2001**, *3*, 31.
(15) Budhani, R. C.; Pant, P.; Rakshit, R. K.; Senapati, K.; Mandal, S.; Pandey, N. K.; Kumar, J. *J. Phys.: Condens. Matter.* **2005**, *17*, 75.
(16) Coey, J. M. D.; Douvalis, A. P.; Fitzgerald, C. B.; Venkatesan, M. *Appl. Phys. Lett.* **2004**, *84*, 1332.
(17) Poul, L.; Jouini, N.; Fiévet, F. *Chem. Mater.* **2000**, *12*, 3123.

Table 1. Chemical Composition of Samples A and B as Deduced from ICP and EDX Analyses

sample	Zn wt %	Co wt %	C wt %	Co/Zn at %[a]
A	59.93	10.22	1.53	19
B	64.20	10.63	0.42	19

[a] Inferred from EDX analysis.

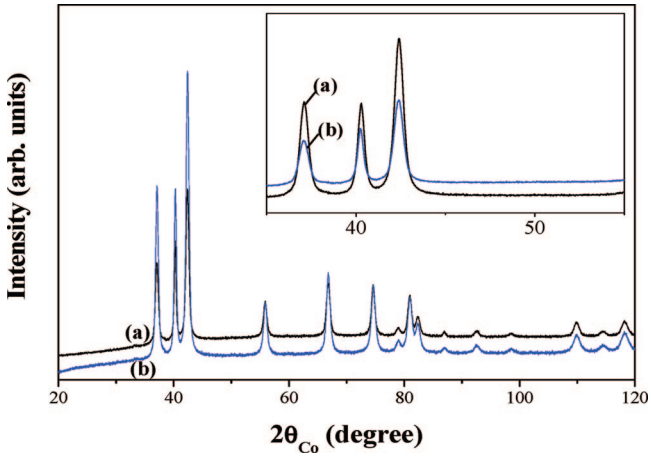

Figure 1. X-ray diffraction pattern of samples (a) A and (b) B. A zoom of the 35−55° 2θ range is given in the inset.

A Quantum Design MPMS-5S SQUID magnetometer was used for magnetic characterization in the 4.2−310 K temperature range. The zero- field-cooled (ZFC) and field-cooled (FC) dc-susceptibility were measured in a magnetic field of 200 Oe. The ZFC isothermal magnetization was also measured at different temperatures from 5 to 300 K by cycling the magnetic field, H, between +10.0 and −10.0 kOe. All the data are given per mol of cobalt.

EPR measurements were performed with a standard X-band (9 GHz) spectrometer in the 4.2−300 K temperature range. For this purpose, small amounts (∼50 mg) of each powder were placed in quartz tubes and inserted into the microwave cavity of the spectrometer. All the spectra have been recorded upon increasing the magnetic field from zero to 8 kOe.

Results

1. Chemical Analysis. As expected, the chemical analysis shows that the Co to Zn concentration ratio of the as-prepared particles is Co/Zn = 0.19, which corresponds to a composition $Zn_{0.84}Co_{0.16}O$ (Table 1). The carbon content in the as-prepared sample is about 1.53 wt. %. Such a carbon contamination is frequently observed in metal and oxide particles prepared in a polyol medium. It is related to acetate and/or polyol molecules adsorbed at the surface of the particles.[18] After heating under N_2 at 400 °C, the carbon content decreases to 0.42 wt % because of the loss of most of the organic species adsorbed at the surface.

2. X-ray Diffraction Analysis. The XRD patterns of samples A and B are given in Figure 1. They show only the wurtzite phase of ZnO. Within the detection limits of this technique, the subsequent thermal treatment does not introduce any additional phase such as Co, CoO, or Co_3O_4 that would have given rise to diffraction peaks between 35 and 65°. This feature suggests that the cobalt atoms are fully incorporated in the ZnO lattice, but as we shall see in the later part of this work, this conclusion is not pertinent. In fact, the absence of additional diffraction peaks in the XRD pattern of sample B will be related to the fact that the Co clusters are too small to be detected by X-ray diffraction spectroscopy.

The position of the XRD diffraction peaks does not change significantly between samples A and B. But the height and width of these peaks do change, which indicates that the heating treatment has modified the shape and size of the particles. The lattice parameters, obtained from a Rietveld refinement, for sample A (a = 3.250(1) Å and c = 5.1936(7) Å) and sample B (a = 3.250(3) Å and c = 5.1955(9) Å) are almost equal and close to those of undoped bulk ZnO (a = 3.249 Å and c = 5.206 Å, JCPDS no. 36−1451). The values of a and c reported in the literature vary with the synthesis conditions and the crystallite size. Some authors report almost the same c-axis lattice parameter as the one of undoped ZnO for $Zn_{1-x}Co_xO$ film.[6] Others report an increase in c with x. To explain this variation, different scenarios have been proposed in the past: the incorporation of interstitial Co ions in the wurtzite lattice,[19] or the formation of Co-vacancy defect complexes.[20] Other authors report a slight decrease in a and c, which they attribute to the small size of the particles. For instance, the lattice parameters of ZnO nanocrystals prepared by the sol−gel route[19] are smaller than those of bulk samples. These authors also found that for low-Co-doped ($x \leq 0.03$) nanocrystals, a unit-cell contraction occurs.[19] This may be rationalized by the different size of Zn^{2+} ions (ionic size 0.60 Å) and Co^{2+} ions (ionic size 0.58 Å).[21] These prior works show that the change of the lattice parameters in Zn(Co)O nanocrystals is not exclusively due to the Co doping and thus cannot be used to quantitatively evaluate the amount of Co incorporated in the ZnO lattice.

The crystallite size L of samples A and B, inferred from the line broadening using the Scherrer formula, is found to be in the nanometer range. The variations of L vs. 2θ for different diffraction lines for sample A (Figure 2a) show that the crystallites of sample A are not isotropic, with the preferential growth direction along the c-axis. The mean crystallite size is 50 nm in the (001) direction and less than 30 nm in the perpendicular direction. In the annealed sample B, the mean crystallite size $L_{(100)}$ has increased, whereas $L_{(002)}$ has decreased (Figure 2b). Thus, the thermal treatment modifies the crystallite shape that becomes more spherical and increases in size.

3. Electron Microscope Study. TEM measurements allow a more detailed analysis of the particle size and shape. Sample A shows submicrometer-sized particles (Figure 3a). All of them have similar shapes and show diameters varying between 400 and 1000 nm. There is no evidence for particles of different morphologies and then of different phases. The TEM observations also reveal that these spherical particles are formed by the aggregation of smaller crystallites, the size

(18) (a) Viau, G.; Fiévet-Vincent, F.; Fiévet, F. *J. Mater. Chem.* **1996**, *6*, 1047. (b) Ammar, S.; Helfen, A.; Jouini, N.; Fiévet, F.; Rosenman, I.; Villain, F.; Molinié, P.; Danot, M. *J. Mater. Chem.* **2001**, *11*, 186.

(19) Hays, J.; Reddy, K. M.; Graces, N. Y.; Engelhard, M. H.; Suttanandan, V.; Luo, M.; Xu, C.; Giles, N. C.; Wang, C.; Thevuthasan, S.; Punnoose, A. *J. Phys.: Condens. Matter.* **2007**, *19*, 266203.

(20) Kim, K. J.; Park, Y. R. *Appl. Phys. Lett.* **2002**, *81*, 1420.

(21) Shannon, R. D. *Acta Crystallogr., Sect. A* **1976**, *32*, 751.

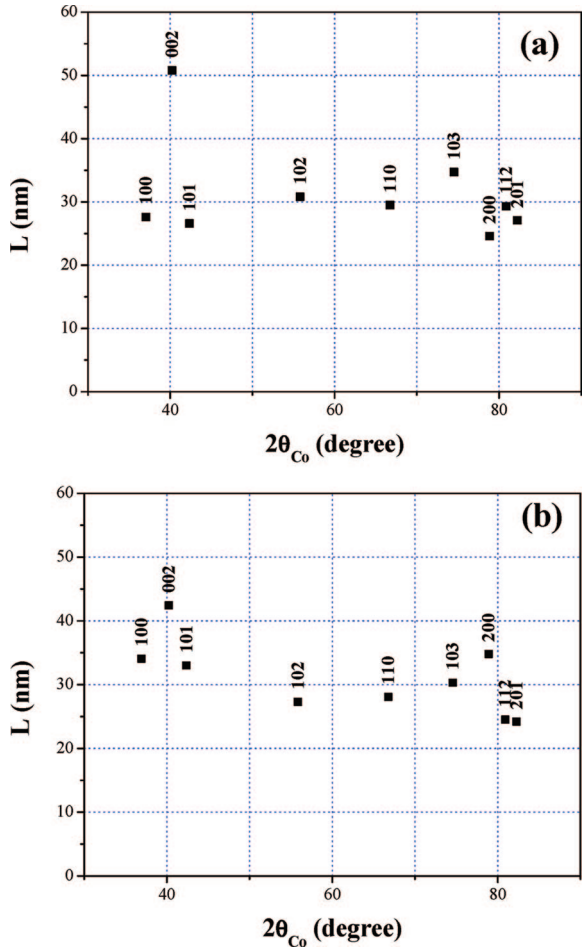

Figure 2. Plot of the crystallite size, L, inferred from line broadening, vs 2θ, for samples (a) A and (b) B.

of which lies in the range of tens of nanometers (Figure 3b), in good agreement with the XRD analysis. A zoom on the border of one representative particle is presented on Figure 3c. It shows rodlike crystallite with a length in the range 50−60 nm and a diameter in the range 10−20 nm. The high-resolution image shows fringes corresponding to crystallographic planes of the hexagonal lattice of the wurtzite structure. The diffraction pattern calculated from the high-resolution image obtained from the selected (white square) area in Figure 3c) corresponds to the ⟨010⟩ zone axis (Figure 3d) with a and c parameters in agreement with XRD results. After heating (sample B), the particles conserve their overall spherical shape and a mean size of about 1 μm (Figure 4a). However, TEM images show that the particles are now made up of a dense packing of nearly spherical crystallites (Figure 4b). The mean crystallite size after thermal treatment is about 40 nm, in good agreement with the calculations inferred from the X-ray line broadening. The selected area electron diffraction (SAED) pattern of one representative particle is completely indexed in the wurtzite structure (Figure 4c), strongly suggesting that the thermal treatment conserves the ZnO phase and does not introduce any secondary phase inside the particles.

4. UV−Visible Absorption. The optical absorption spectra of samples A and B are given in Figure 5. The analysis of the spectra in the UV spectral region is made difficult by the diffusion effects of the powder samples. They give rise

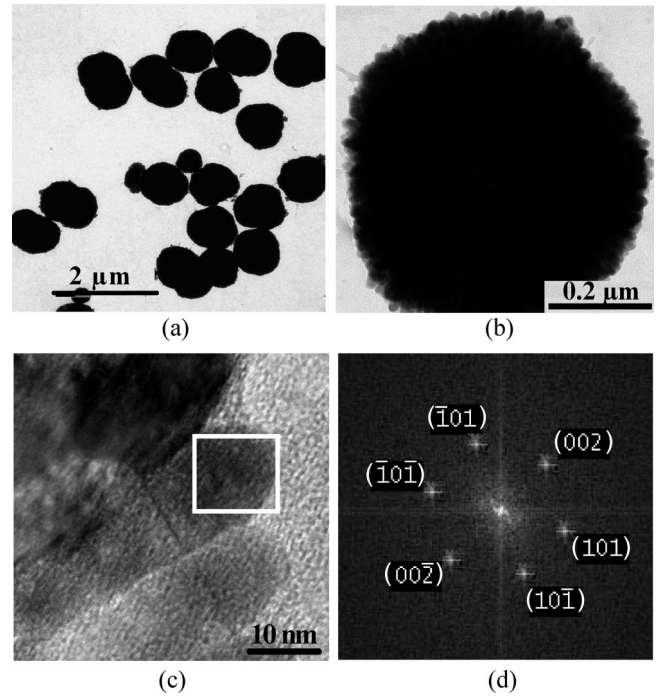

Figure 3. TEM images of an assembly of (a) as-produced particles, (b) one representative particle, (c) a zoom on its border and (d) the FFT pattern of a selected area.

to an increasing background absorption starting at 500 nm. To obtain the energy gap E_g, we have performed a Kubelka−Munk (KM) analysis (see for instance ref 22), using the KM function $\Phi(R) = (1 - R)^2/(2R)$ with R the diffuse reflectance. According to this model, $(\Phi(R)h\nu)^2$ vs photon energy $h\nu$ will show a linear region just above the optical absorption edge, which is well-observed experimentally as can be seen in the inset of Figure 5. The extrapolation of the linear part ($E > 3.5$ eV) gives a value of $E_g = 3.25$ eV for sample A. This is only slightly smaller than that of bulk ZnO (3.30 eV).[23] A small decrease in E_g with increasing the Co content has been reported before for $Zn_{1-x}Co_xO$ films with $x \leq 0.15$ grown on Al_2O_3 (001) substrates by pulsed laser deposition,[24] or by rf magnetron sputtering.[20] In these cases, the band gap narrowing upon increasing x has been attributed to the sp−d exchange interactions between the band electrons and the localized d electrons of the substituted Co^{2+} ions. Moreover, magneto-optical measurements performed on various $Zn_{1-x}M_xO$ materials, where M is a divalent transition metal, have evidenced a large magneto-optic effect in $Zn_{1-x}Co_xO$, the largest observed, indicating strong exchange interaction between the sp band electrons and the localized d electrons.[25]

The visible and IR domain of the absorption spectra (figure 5) is dominated by the crystal field transitions of substitutional Co^{2+}_{Zn} ions.[26] The spectra display two main bands that were previously attributed to the $^4A_2 \rightarrow {}^4T_1(P)$ and $^4A_2$

(22) Kortum, G., *Reflectance Spectroscopy*; Springer-Verlag: New York, 1969.
(23) Srikanf, V.; Klarke, D. R. *J. Appl. Phys.* **1998**, *83*, 5447.
(24) Samanta, K.; Bhattacharya, P.; katyiar, R. S. *Appl. Phys. Lett.* **2005**, *87*, 101903.
(25) Ando, K.; Saito, H.; Jin, Z.; Fukumura, T.; Kawasaki, M.; Matsumoto, Y.; Koinuma, H. *J. Appl. Phys.* **2001**, *89*, 7284.
(26) Koidl, P. *Phys. Rev. B* **1977**, *15*, 2493.

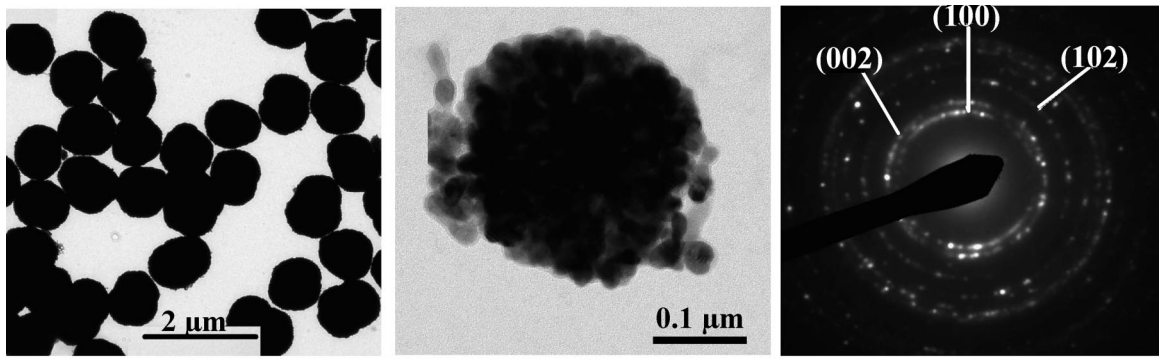

Figure 4. TEM images of an assembly of (a) the heated-in-nitrogen particles, (b) one representative particle, and (c) its SAED pattern.

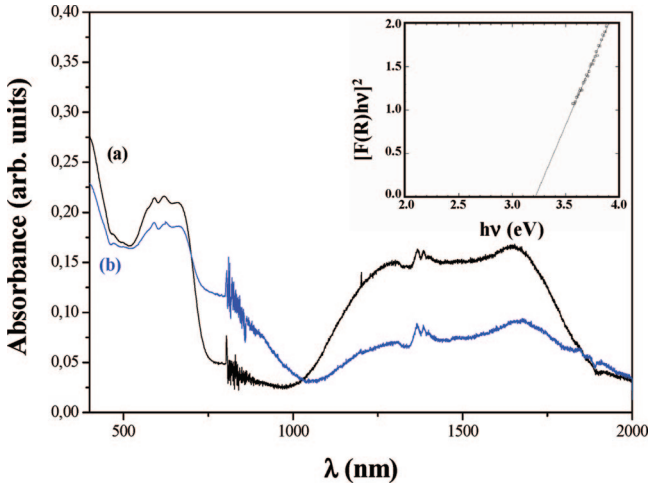

Figure 5. Absorption spectra of samples (a) A and (b) B. The Tauc plot is shown in the insert to measure the gap of sample A. Note the noise observed in the spectra around 800 nm is due to detector change.

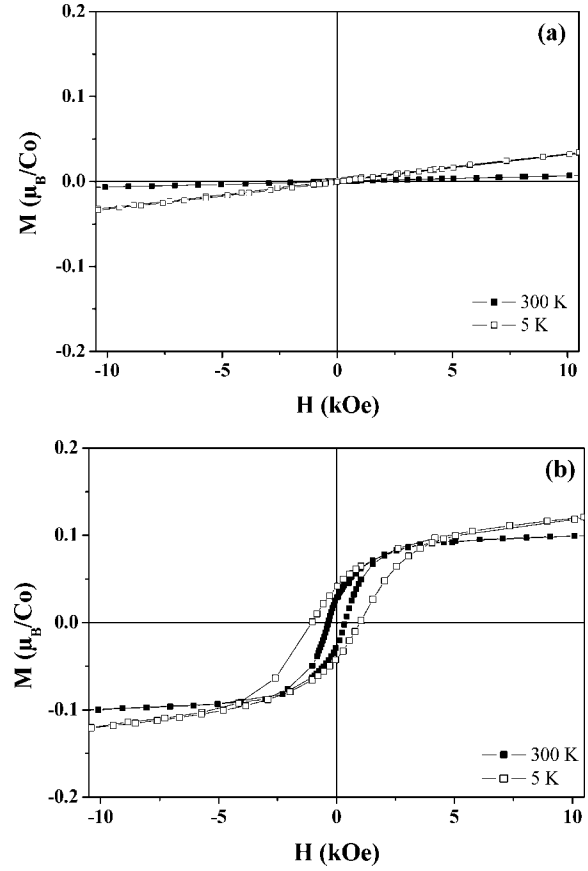

Figure 6. Magnetization curves of samples (a) A and (b) B at temperatures 5 and 300 K.

→ $^4T_1(F)$ transitions of Co^{2+}. Each band contains different subbands at 659, 619, and 570 nm and at 1311, 1388, and 1655 nm, respectively, related to the spin−orbit splitting of the 3d states. Similar results for $Zn_{1-x}Co_xO$ have been reported for thin films[20,27,28] and powders.[14,19] As the absorption coefficient has not been calibrated in absolute units, we cannot deduce the value of the Co-composition from these spectra. On another hand, the scaling factor can safely be assumed to be the same for both the samples A and B. As the spectra of Figure 5 show a 50% decrease in the Co^{2+} absorbance after the thermal annealing, we can conclude that the concentration of the substitutional Co^{2+} has decreased by a factor of 2 because of the heat treatment.

5. Magnetic Measurements. The magnetization curve $M(H)$ of the as-prepared and heat-treated samples was measured at 5 and 300 K. Sample A is paramagnetic, as established by the linear variation of M with the magnetic field for temperatures between 5 and 300 K (Figure 6a). There is neither any hysteresis nor remnant magnetization at any temperature; the sample is paramagnetic down to 5 K. This feature is confirmed by the monotonous variation of the dc-susceptibility χ as a function of the temperature in a low magnetic field of 200 Oe, and by the linear variation of its reciprocal function, $\chi^{-1}(T)$ at high temperature where the Curie−Weiss law is obeyed (Figure 7a). A deviation from the Curie law is, however, observed at low temperature (below 50 K). This can be due to a small concentration of Co ions not incorporated in the ZnO matrix, giving a contribution of uncorrelated spins to χ that increases in T^{-1} at low temperature. The concentration of such loose spins, however, is smaller than 1 at %, so that sample A can be considered as a sample of chemical formula $Zn_{0.84}Co_{0.16}O$. The linear fit of $\chi^{-1}(T)$ by the Curie−Weiss law in the 100−310 K range allows us to determine the effective magnetic moment, μ_{eff}, of 5.1 μ_B/Co, and the paramagnetic Curie temperature $\theta_p = -90$ K. As expected, the value of μ_{eff} is intermediate between the spin-only value (3.87 μ_B)

(27) Ramachndran, S.; Tiwari, A.; Narayna, J. *Appl. Phys. Lett.* **2004**, *85*, 5255.
(28) El Mir, L.; Ben Mahmoud, A.; von Bardeleben, H. J.; Cantin, J. L. *Mater. Res. Soc. Symp. Proc.* **2007**, *957*, K10.

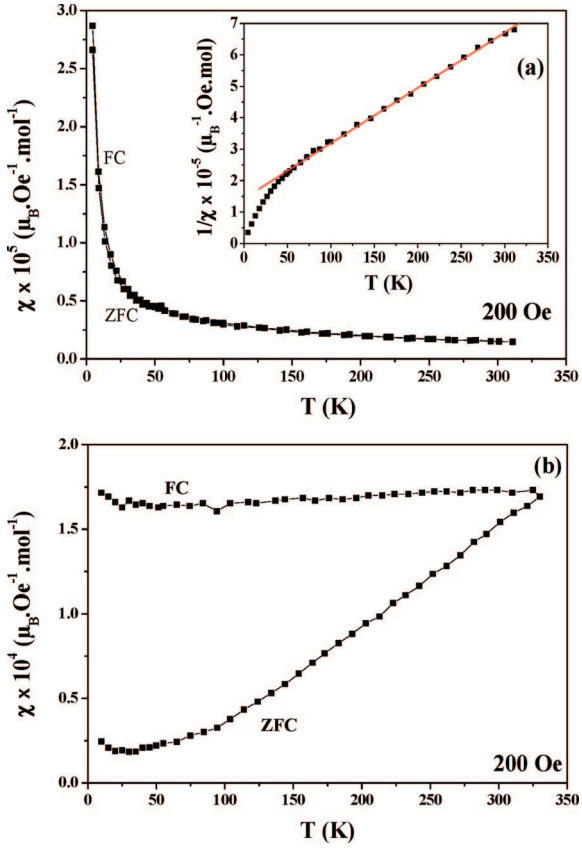

Figure 7. Temperature dependence of the FC- and ZFC-susceptibility χ measured on samples (a) A and (b) B. In this figure, χ is defined as the ratio M/H with M the magnetization measured in an applied field of 200 Oe. The curve $1/\chi(T)$ is given in the inset for sample A to illustrate the Curie−Weiss behavior at high temperature.

and the free Co^{2+} ion value (6.63 μ_B). Indeed, the orbital momentum of Co^{2+} is usually only partially quenched by the crystal field, and the mean value of the effective magnetic moment carried by tetrahedrally coordinated Co^{2+} in solids is 4.80 μ_B[29]. The absence of magnetic ordering at such a composition $x = 0.16$ that is close to the percolation threshold for nearest-neighbor (nn) interaction gives evidence that the magnetic interactions are short-range, and dominated by the nn superexchange interactions that are antiferromagnetic. We did not investigate the possibility of spin glass freezing at low temperature. The spin glass freezing, even if it exists, will be masked by the loose spin contribution to the magnetic susceptibility that diverges in T^{-1} at low temperature, and thus becomes dominant at low temperature where this spin-glass freezing is expected to take place.

Sample B, which had been heated in nitrogen, shows quite different magnetic properties at low and at room temperatures. The $M(H)$ curve measured at 5 K (Ffigure 6b) exhibits a ferromagnetic component, characterized by a hysteresis with a coercivity of 1.05 kOe and a remanant magnetization of 0.04 μ_B/Co. We use the conventional notation μ_B/Co of Bohr magneton per cobalt atom, based on the amount of cobalt measured by the chemical analysis (Table 1). Of course, this approach implicitly assumes that all the cobalt atoms are substituted as Co_{Zn} in the ZnO lattice, and this will be questioned later on in this work. Nevertheless, we keep for the moment this unit to make contact with earlier works that used it. In magnetic field of 10 kOe, the magnetization reaches a value of 0.12 μ_B/Co. The coercivity, the remanant magnetization, and the magnetization at 10 kOe decrease only slightly at 300 K to 0.38 kOe, 0.03 μ_B/Co and 0.10 μ_B/Co, respectively. For clarity, all these values are summarized in Table 2. The magnetization measured at 10 kOe is of the same order of magnitude as the values reported recently for Mn^{2+}:ZnO pellets,[2] for Ni^{2+}:ZnO nanocrystalline aggregates[30,31] and for Co^{2+}:ZnO.[11,30] It must be stressed that this magnetization is much weaker than the spin-only moment of Co^{2+} ions in the high-spin d^7 configuration $e^4t_2^3$ (about 3 μ_B/Co). The small 300 K coercivity and the resulting small hysteresis area are very similar to those of other ferromagnetic ZnO DMS powders.[2,3,11,30,32] Moreover, the coercivity is found to decrease when increasing the temperature, just like in other ZnO based DMS.[2,5,33] Therefore, the magnetic properties allow us to conclude that thermal annealing at 400 °C under N_2 generates a ferromagnetic component in the Zn(Co)O powders. It should be noted that all the claims for ferromagnetism in transition-metal-doped ZnO have been reported so far in n-type conductive materials.[11,32,34]

Table 2. Magnetization at $H = 10$ kOe (M_{10kOe}), Remanent Magnetization (M_r), and Coercitivity (H_C) at $T = 5$ and 300 K for Samples A and B

sample	$M_{10\ kOe}$ (5 K) μ_B/Co	M_{10kOe} (300K) μ_B/Co	M_r(5 K) μ_B/Co	M_r (300 K) μ_B/Co	H_c (5 K) Oe	H_c (300 K) Oe
A	0.032	0.007	0	0	0	0
B	0.12	0.10	0.04	0.03	1050	380

The variation of the FC- and ZFC-susceptibility, χ, as a function of the temperature in a low magnetic field of 200 Oe of sample B is characteristic of ferromagnetic nanoparticles with a blocking temperature higher than 300 K (Figure 7b). The existence of Co particles small enough so that their blocking temperature is smaller than room temperature is likely, but it is impossible to detect them by magnetic experiments, even if they exist. The reason is that broad distribution of the sizes of the particles means broad distribution of blocking temperatures, which in turn only results in an increasingly large difference between field cooled and zero-field-cooled experiments. This effect, however, cannot be distinguished from the increasingly large difference between field-cooled and zero-field-cooled experiments resulting from the slower dynamics of the magnetic moment orientation of the bigger particles. In other words, the magnetic measurements can probe the onset of magnetic irreversibility, which corresponds to the blocking of the largest particles only. The size distribution of ferromagnetic

(29) Kittel, C., *Introduction to Solid State Physics*. Dunod: Paris, 1970).
(30) Radovanovic, P. V.; Gamelin, D. R. *Phys. Rev. Lett.* **2003**, *91*, 157202.
(31) Schwartz, D. A.; Kittilstved, K. R.; Gamelin, R. *Appl. Phys. Lett.* **2004**, *85*, 1395.
(32) Schwartz, D. A.; Norberg, N. S.; Nguyen, Q. P.; Parker, J. M.; Gamelin, D. R. *J. Am. Chem. Soc.* **2003**, *125*, 13205.
(33) Cho, Y. M.; Choo, W. K.; Kim, H.; Kim, D.; Ihm, Y. *Appl. Phys. Lett.* **2002**, *120*, 439.
(34) (a) Kittilstved, K. R.; Norberg, N. S.; Gamelin, D. R. *Phys. Rev. Lett.* **2005**, *94*, 147209. (b) Goennenwein, S. T. B.; Wassner, T. A.; Huebl, H.; Brandt, S. M.; Philipp, J. B.; Opel, M.; Gross, R.; Koeder, A.; Schoch, W.; Waag, A. *Phys. Rev. Lett* **2004**, *92*, 227202.

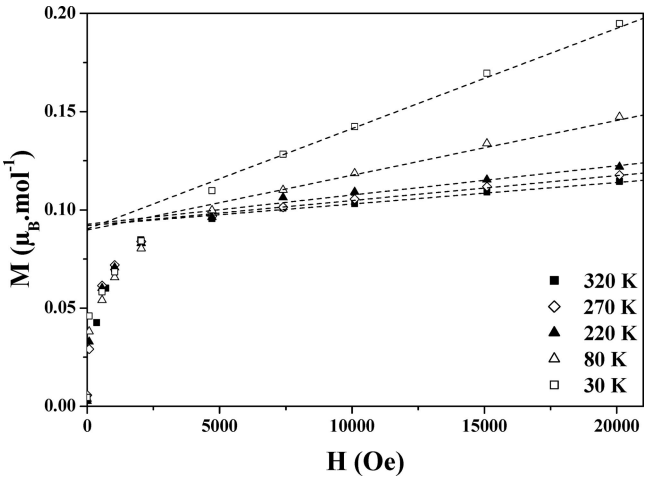

Figure 8. First magnetization $M(H)$ curves of sample B measured at different temperatures. Note thatall the tangents to the magnetization curves at $H =$ 20 kOe (broken lines) intercept the ordinate axis at the same point, which defines the magnetization $M_0 = 0.09\ \mu_B$/Co.

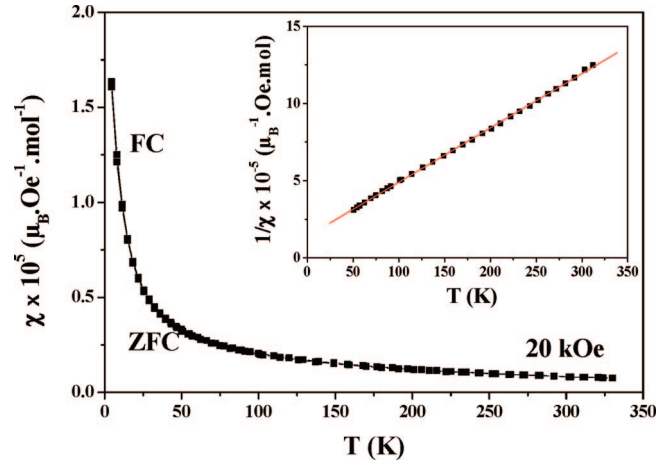

Figure 9. Intrinsic part of the magnetic susceptibility of sample B, defined according to $\chi(T) = (M - M_0)/H$ with with M the magnetization measured as a function of temperature at a magnetic field of $H = 20$ kOe and M_0 defined in Figure 8. A zoom of the $1/\chi(T)$ curve at high temperature is given in the inset. The continuous line is a fit according to the Curie−Weiss law.

particles can be accessed only in some particular cases, from the fit of the magnetization curves above the blocking temperature of all the particles.[35] In the present case, however, this range of temperature cannot be accessed because of the biggest particles are already frozen at room temperature.

The extrinsic nature of the ferromagnetic component can be directly inferred from an analysis of the $M(H)$ curves which can be decomposed in two parts. The first one is an intrinsic componant $\chi(T)H$ that is linear in field. The other one is an extrinsic component that represents the contribution of the ferromagnetic nanoparticles. These particles act as macro-spins so that their magnetization is easily saturated by application of an external field of about 5 kOe. Let us call M_0 this magnetization at saturation of the ferromagnetic nanoparticles. The total magnetization for fields $H > 5$ kOe can then be written in the form:

$$M = M_0 + \chi(T)H \quad (H > 5\ \text{kOe}) \tag{1}$$

This is illustrated in Figure 8. The magnetization M_0 can be obtained by extrapolation to $H = 0$ of the part of the magnetization curve that is linear in H for $H > 5$ kOe. The result is

$$M_0 = 0.09\ \mu_B/\text{Co} \tag{2}$$

The value of M_0 is independent of T, which means that the nanoclusters are made of a material that is ferromagnetic with a Curie temperature higher than room temperature. This feature indicates the presence of metallic Co clusters. From eq 1, we have deduced the intrinsic magnetic susceptibility from the relation

$$\chi(T) = (M - M_0)/H \quad (H > 5\ \text{kOe}) \tag{3}$$

with M the magnetization measured as a function of temperature at a magnetic field of $H = 20$ kOe. The result is reported in Figure 9 under the form of $\chi(T)$. The Curie−Weiss law is again satisfied above 100 K just like in the case of sample A. The difference, however, is that both the Curie constant and θ_p are twice smaller that in sample A. Thus, the concentration x of the Co ions in substitution to Zn has decreased by a factor two, in agreement with the result deduced from the analysis of the optical spectra: Sample B is thus a mixture of $Zn_{0.92}Co_{0.08}O$ particles and metallic Co-nanoclusters. The main effect of the thermal treatment has then been the segregation of the cobalt under the form of Co-nanoclusters that have grown at the expense of the cobalt incorporated in the ZnO matrix.

From the relation $\theta_p = \theta_0 x$ we obtain a value of $\theta_0 = -562.5$ K. It is more difficult to deduce from θ_0 an estimate of the nn superexchange interaction here than in the case of $Zn_{1-x}Mn_xO$ as the orbital momentum is not entirely quenched; this implies the existence of an important single-ion anisotropy that affects the expression of θ_p. Nevertheless, an estimation of the nn superexchange integral averaged over the angular variables, J, can be obtained by the simplified expression

$$J = \frac{6k_B\theta_0}{z(\mu_{\text{eff}}/\mu_B)^2} \tag{4}$$

where $z = 12$ is the number of nearest neighbors (no distinction has to be made here between the nonequivalent axial and nonaxial neighbors, since we have averaged over the angular variables). In case the magnetic ions carry a spin S and no orbital momentum (case of Mn^{2+}), $(\mu_{\text{eff}}/\mu_B)^2 = 4S(S+1)$. Equation 4 with this expression of μ_{eff} has been successfully used to estimate J in $Zn_{1-x}Mn_xO$,[4] in agreement with magnetization step measurements at high field and low temperature. Equation 4 is the trivial extension to the $Zn_{1-x}Co_xO$ case where the magnetic ion also carries an orbital momentum that is not completely quenched. With the values $\mu_{\text{eff}} = 5.1\ \mu_B$ and $\theta_0 = -562.5$ K derived in the present work, we find $J/k_B = -10.8$ K. This value is in agreement with a recent analysis of the magnetization curves at low temperature of $Zn_{1-x}Co_xO$ with smaller Co concentrations ($x \leq 0.07$),[36] according to which the nn exchange constant is antiferromagnetic and exceeds 10 K (in absolute value).

(35) Berret, J.-F.; Sandre, O.; Mauger, A. *Langmuir* **2007**, *23*, 2993.

(36) Sati, P.; Deparis, C.; Morhain, C.; Schäfer, S.; Stepanov, A. *Phys. Rev. Lett.* **2007**, *98*, 137204.

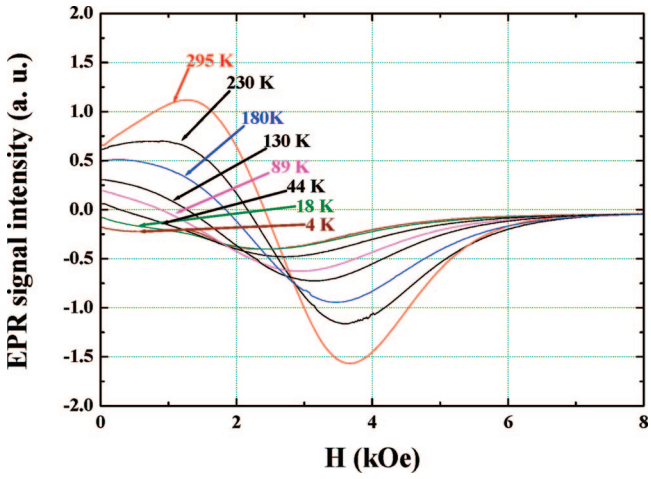

Figure 10. EPR spectra of sample B measured at different temperatures between 295 and 5 K.

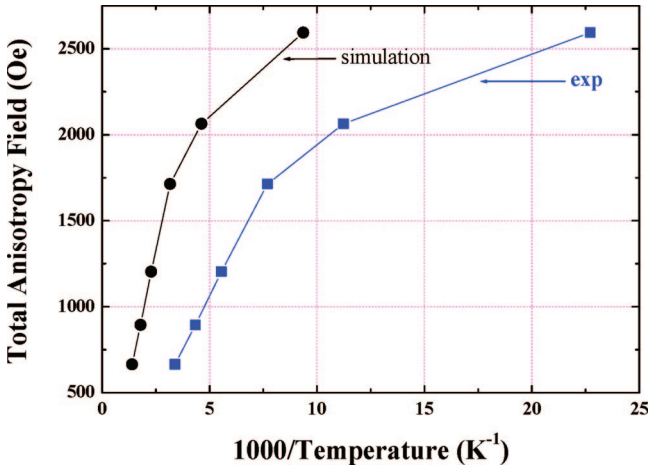

Figure 11. Simulated (black squares) and experimental (blue circles) total ansisotropy fields as a function of 1000/T for sample B; the simulation parameters are a particle diameter $r = 2$ nm, an applied magnetic field of 1 kOe, and a magnetization of 1700 erg/Oe cm^3.

Therefore, in $Zn_{1-x}Co_xO$ like in $Zn_{1-x}Mn_xO$, there is a self-consistency in the evaluation of the antiferromagnetic nn interactions from high temperature magnetic susceptibility and from low-temperature magnetization curves, at all concentrations up to the percolation threshold $x_c = 0.16$ (we have argued elsewhere that the simple relation $\theta_p \propto x$ is observed only at $x \leq x_c$).[4] $Zn_{1-x}Co_xO$ is thus a regular diluted magnetic semiconductor with antiferromagnetic superexchange interactions, just like $Zn_{1-x}Mn_xO$, or any other Mn-based II−VI compound.[4]

6. Electron Paramagnetic Resonance Experiments. At room temperature, the two samples A and B show the same EPR spectrum, but with very different intensities. This spectrum is different from the powder spectrum of substitutional Co^{2+} in ZnO. Such a spectrum is observed neither at room temperature nor at low temperature. The fact that it is not observed at room temperature is not surprising, because the excessive line broadening above $T = 100$ K makes the very anisotropic EPR spectrum of isolated Co^{2+} in ZnO difficult to observe.[13] At low temperature, the reason is the excessive dipolar line broadening and its anisotropic character with $g_{\perp c} = 4.20$ and $g_{\parallel c} = 2.01$. The intensity of the spectrum observed at room temperature in sample B (Figure 10) is approximately 2 orders of magnitude higher than that of sample A. At $T = 300$ K, it is characterized by a broad asymmetric line with an effective g-factor of 2.70 and a line width of ∼2500 Oe. This spectrum does not correspond to that of Co^{2+} in ZnO. It is very temperature dependent: its resonance field decreases and the line width increases strongly upon cooling to $T = 4$ K. Such a temperature dependence, as well as the shape and line width of the spectrum, are the signature of magnetic nanoparticles.[37] As we shall see below, the attribution of the magnetic particles to metallic Co clusters allows a simple interpretation of our results. In this framework, the temperature dependence of the EPR spectrum can be understood by the combined effect of temperature-dependent demagnetization and anisotropy fields.[37] Its basic properties can be quantitatively reproduced in the simple model of an ensemble of noninteracting elliptical magnetic particles of identical size. In this case, the resonance position will be given by[37]

$$H_{res} = H_0 + H_{aniso} + H_{demag} \quad (5)$$

H_0 is the resonance field expected from the Landé g-factor, which is $g = 2.15$ for metallic Co. H_{aniso} is the magnetocrystalline anisotropy field and H_{demag} the demagnetizing field related to the shape anisotropy of the particles. Given their small concentration, the clusters are assumed to be noninteracting. The demagnetization field varies with temperature according to the equation

$$H_{demag} = \Delta N M_s(\coth x - x^{-1}) \quad (6)$$

wereas $x = (M_s VH)/(kT)M_s$ is the magnetization density of metallic cobalt at saturation, V the volume of the nanoparticles (supposed to be monodisperse for simplicity), H the applied magnetic field, k the Boltzman constant, and T the temperature. ΔN is a shape form factor. The variation in the anisotropy fields with temperature will be different for cubic and uniaxial crystal symmetries.[37] In case of uniaxial anisotropy

$$H_{aniso} = H^0_{aniso}\frac{1 - 3x^{-1}\coth x + 3x^{-2}}{\coth x - x^{-1}} \quad (7)$$

whereas in the cubic case it takes the form

$$H_{aniso} = H^0_{aniso}\frac{1 - 10x^{-1}\coth x + 45x^{-2} - 105x^{-3}\coth x + 105x^{-4}}{\coth x - x^{-1}} \quad (8)$$

Because the magnetic clusters are generated during the heating at 400 °C, the metallic cobalt clusters should be crystallized in its stable phase of this element, namely the hexagonal phase, in which case $H^0_{aniso} = 1.056$ T and $M_s = 1700$ erg Oe^{1-} cm^{-3}. We can then simulate the temperature variation of the resonance fields quantitatively by choosing the shape anisotropy form factor $\Delta N = 0.25$ (Figure 11). This result, together with the optical absorption and SQUID measurements allow us to conclude that we are dealing with metallic Co particles. As metallic Co precipitates are known

(37) de Biasi, R. S.; Devezas, T. C. *J. Appl. Phys.* **1978**, *49*, 2466.

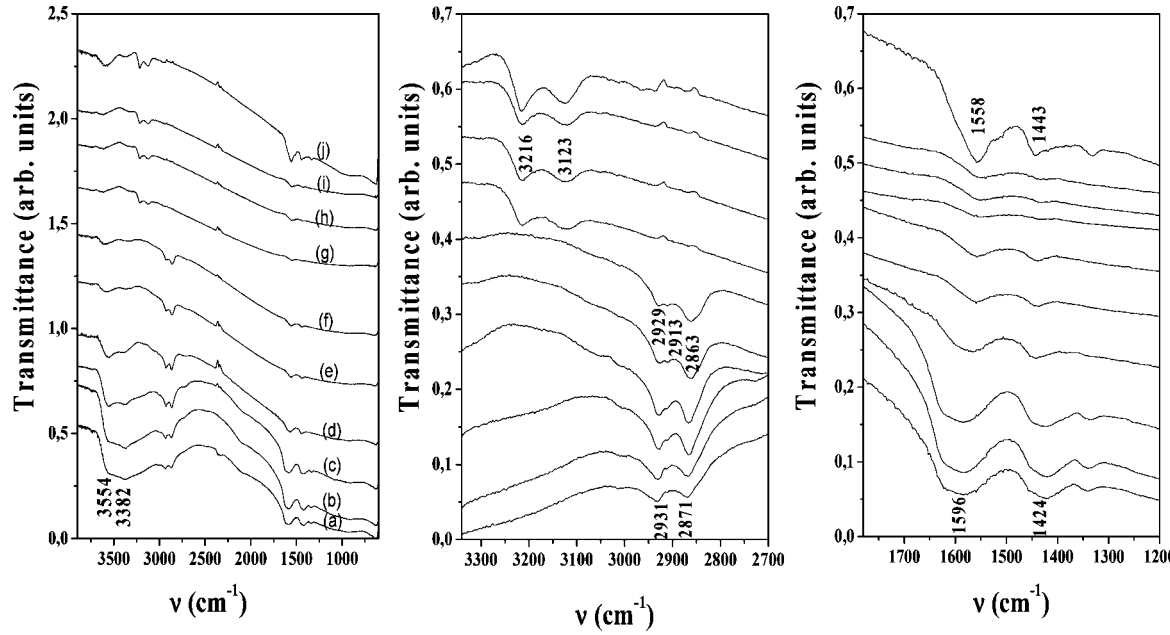

Figure 12. In situ temperature-resolved IR spectra of the as-produced particles upon heating step-by-step at (a) 25, (b) 50, (c) 100, (d) 150, (e) 200, (f) 250, (g) 300, (h) 350, and (i) 400 °C and (j) after cooling at 25 °C. The sample stayed at each temperature for the time (∼1 h) needed to perform the IR experiment. Note that the gas residue formed during the thermal decomposition of the initially adsorbed organic species was still present in the sampling cell. For clarity, the spectra were voluntary vertically shifted and presented in three vibration energy ranges: (a) from 3800 to 800 cm^{-1} (left), to give a view of the whole spectra; (b) from 3350−2700 cm^{-1} (center), to zoom on the OH and CH_2 bands; and (c) from 1775 to 1200 cm^{-1} (right), to zoom on the COO bands.

to be a frequent contamination in highly doped Co:ZnO powders and films,[38] the EPR results can be taken as an additional indication for their presence in the annealed powders.

7. Thermal Treatment Survey. We have recorded the IR transmission spectrum of the as-produced particles (Figure 12). The analysis of the spectrum confirms the presence of organic species previously detected by chemical analysis. It clearly shows the presence at the surface of these particles of (i) acetate ions, characterized by the specific symmetric and asymmetric ν(CO) vibration bands at 1596 and 1424 cm^{-1}, respectively; (ii) diethyleneglycol, characterized by the ν(OH) band at 3382 cm^{-1} and $\nu(CH_2)$ vibration bands at 2931−2971 cm^{-1}; and (iii) water, characterized by the ν(OH) at 3350 cm^{-1}. The expected band around 1600 cm^{-1} arising from the $\delta(H_2O)$ bending mode is hidden by the relatively strong band at 1500−1600 cm^{-1} due to the CO asymmetric stretching mode, as observed in previous work on hydrated metal acetates.[39]

The thermogravimetric analysis (TGA) of the as-produced particles (sample A) performed in a nitrogen atmosphere is given in Figure 13. It exhibits two important weight losses. The final products of decomposition can be considered as representative of sample B, because the magnetization curve at room temperature (not shown here) include a ferromagnetic component, with the same characteristics (H_c, M_r, M_{sat}) as those of sample B.

The first weight loss is endothermic and occurs close to T = 100 °C. It is attributed to desorption of physisorbed water. The second weight loss is exothermic and occurs in the 300−400 °C temperature range. To identify the chemical

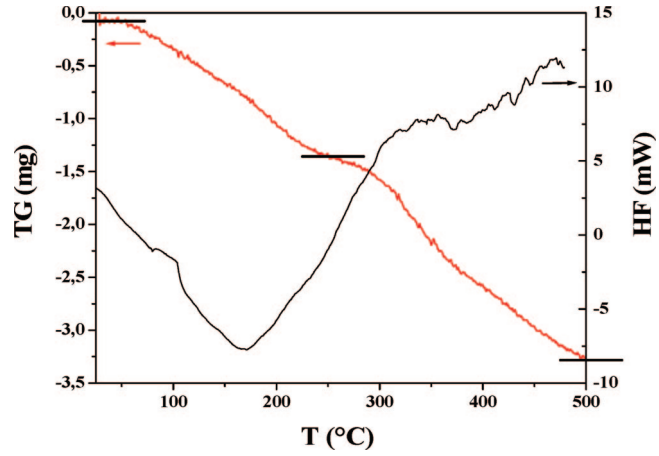

Figure 13. Temperature dependence of the mass loss (TG) and the heat flow (HF) for the as produced particles during thermogravimetric analysis in nitrogen. The horizontal lines delimit the two main weight losses.

species involved in this reaction, a TGA analysis in argon up to 600 °C coupled with mass spectrometry has been performed (the change of the gas, from nitrogen to argon, shifts the thermal transformations to higher temperatures). Up to 100 °C only water is detected (molecular peak at 18 g mol^{-1}), and between 300 and 600 °C a series of different molecular peaks is detected. The most important ones correspond to masses of 2, 18, 28 and 44 g mol^{-1} that correspond to H_2, H_2O, C_2H_4, and/or CO, and CO_2 species, respectively (Figure 14). Another peak corresponding to 43 g mol^{-1} remains unidentified. These species are related to the exothermic decomposition of the diethyleneglycol and/or acetate.

In situ IR transmission spectra were measured for sample A in order to further analyze the desorption process. They show that some species, diethyleneglycol certainly and

(38) Rode, K. PhD Thesis, University of Paris Sud, Paris, 2006.
(39) Baraldi, P.; Fabbri, G. *Spectrochim. Acta* **1981**, *37A*, 89.

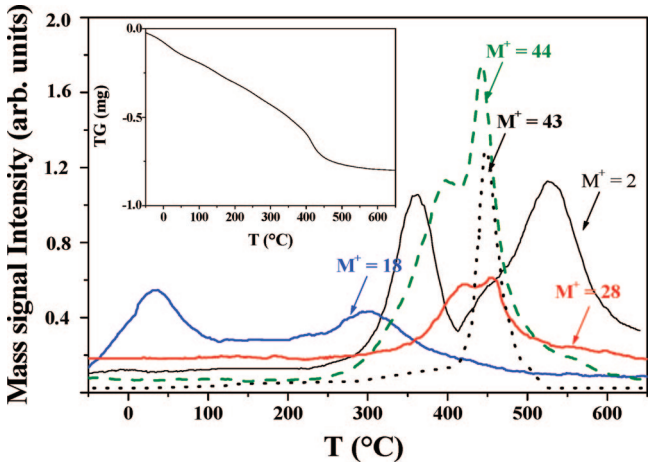

Figure 14. Thermogravimetric analysis in argon (in the inset) coupled with mass spectrometry for the as produced particles.

acetate probably, break down between 300 and 400 °C. Indeed, the spectra recorded in situ, under static nitrogen gas in a transparent airtight cell, at 25, 50, 100, 150, 200, 250, 300, 350, and 400 °C followed by a cooling to 25 °C (Figure 12), give evidence that the specific vibration bands of diethyleneglycol, namely ν(OH) and $\nu(CH_2)$ observed at 3382 and 2931−2971 cm^{-1}, respectively, decrease in intensity upon heating up to 300 °C. These bands are no longer observed above 300 °C. Moreover, the formation of ethylene groups, which results from the degradation of diethyleneglycol, is also established by the IR spectra recorded at 300, 350, and 400 °C, and by the presence of the specific vibration υ(CH) bands at 3216 and 3123 cm^{-1}. Acetate species also appear to be affected by the heating process. The difference $\Delta\upsilon = \nu_{as}(CO) - \nu_s(CO)$ decreases from 172 to 110 cm^{-1} on heating to 300 °C. This decrease can correspond to a modification of the molecular symmetry of acetate ions from a coordinated form to a free one.[40] However, no peak with a molecular weight close to that of acetate or acetic acid is observed in the previous mass spectrometry analysis, and none of the vibration bands of the CH_3 group is observed in the IR spectra up to 300 °C. For this reason, we attribute the bands at 1558 and 1443 cm^{-1} observed up to 300 °C to residual organic species still adsorbed at the surface of the particles, in relation to a probable exothermic decomposition of acetate. A careful examination of the relevant literature allows us to identify them. Such bands are usually assigned to reactive CO_2 adsorbed at the surface of ZnO. They are assigned to carboxylate (CO_2 linked to the surface by its carbon atom) and symmetrical noncoordinated carbonate species, respectively,[41] confirming our hypothesis of residual organic species still adsorbed at the surface of the particles below 300 °C. Moreover, a previous study devoted to the desorption process of acetate from the surface of crystalline nanometer-sized ZnO particles prepared by sol−gel route has shown that, in the absence of oxygen (under argon), a reductive decomposition is favored, leading to fragments of CH_3 (molecular peak of 15), CH_3COO (molecular peak of 59) and CH_3COOH (molecular peak of 60) detected by mass spectrometry at temperature between 300 and 400 °C.[42] This study also points out that this decomposition is not complete, since the absolute content of acetate, determined by elemental analysis of ZnO sample dried in vacuum, was lowered by only about 63% after heating. Another study has shown that acetate species strongly bind to the surface of crystalline micrometer-sized ZnO particles prepared by ceramic process desorbed under vacuum in a complex fashion involving, between 300−400 °C, ketene (CH_2CO), acetic acid (CH_3COOH), CO_2, H_2, and water.[43] These products were identified by mass spectrometry, acetic acid being "fingerprinted" by large peak of m/e = 60, 45, 43, and 15. The authors also suspected that part of the carboneous residue remained adsorbed on the solid phase. The desorption of acetate from the surface of crystalline ZnO clearly depends on the sample preparation. However, in all the cases, it occurs between 300 and 400 °C in absence of O_2, and leads to the formation of smaller molecules such as CO_2, which remained partly adsorbed at the surface.

In conclusion, TG analyses coupled with mass spectrometry and completed by temperature-resolved IR spectroscopy conducted on sample A show that the particles produced in polyol are capped by adsorbed water, diethyleneglycol and acetate species. Upon heating to 300−350 °C, these molecules depart from the surface of the particles and decompose into smaller molecules. This is particularly the case of diethyleneglycol, which leads to the formation of CO_2, H_2O, C_2H_4, and H_2 species, without excluding CO even if its presence is not clearly evidenced in the IR spectra. The boiling point of diethyleneglycol is about 250 °C. Its departure at higher temperature (between 300 and 350 °C) in a decomposed form suggests that it is chemisorbed. It is also very probably the case of acetate whose decomposition should induce the formation of CO_2, H_2, and H_2O, and even if some residual organic species are still attached to the surface of the heated particles, in agreement with a close to zero but nonzero carbon content measured on sample B, they are non-oxygen-coordinated.

Discussion

Magnetic measurements have clearly shown that intrinsic $Zn_{1-x}Co_xO$ is a diluted magnetic semiconductor with antiferromagnetic superexchange interactions like $Zn_{1-x}Mn_xO$. This was actually expected since the exchange interactions between high-spin tetrahedral coordinated Co^{2+} ions in the hexagonal lattice of the wurtzite structure are the short-range $Co^{2+}-O-Co^{2+}$ superexchange interactions that are antiferromagnetic according to the well-known Goodenough−Kanamori rules. These results are then in agreement with several studies of $Zn_{1-x}Co_xO$ with $x < 0.20$[44] that had shown Curie−Weiss behavior with a negative Curie paramagnetic temperature.

(40) Nakamoto, K., *Infrared and Raman Spectra of Inorganic and Coordination Compounds*, 4th ed.; John Wiley and Sons: New York, 1986.
(41) Busca, G.; Lorenzelli, V. *Mater. Chem.* **1982**, *7*, 89. and the references therein. .
(42) Noack, V.; Eychmüller, A. *Chem. Mater.* **2002**, *14*, 1411.
(43) Bowker, M.; Houghton, H.; Waugh, K. C. *J. Catal.* **1983**, *79*, 431.
(44) (a) Yoon, S. W.; Cho, S. B.; We, S. C.; Yoon, S.; Suh, B. J.; Song, H. K.; Shin, Y. J. *J. Appl. Phys.* **2002**, *93*, 7879. (b) Bouloudenine, M.; Viart, N.; Colis, S.; Kortus, J.; Dinia, A. *Appl. Phys. Lett.* **2005**, *87*, 52501.

For lower doping levels, a ferromagnetic Curie−Weiss behavior has also been reported, but no long-range order exists in such samples at temperatures ≥4 K.[13]

Ferromagnetism has been induced in our samples by heating at 400 °C, and we have shown that this is an extrinsic property due to the formation of magnetic particles with the properties expected for metallic Co-clusters. Because, however, many prior works interpreted similar data as an evidence of intrinsic ferromagnetism in these materials, it may be desirable to discuss in more details the origin of this misunderstanding. On the basis of density function calculations, it was recently argued that, whereas p-type doping in $Zn_{1-x}Co_xO$ could produce a stable ferromagnetic state, oxygen vacancies, and the resulting n-type conductivity should stabilize an antiferromagnetic state.[45] Indeed, due to the different strengths of the interactions, the two kinds of doping are not equivalent. In p-type materials, the p−d hybridization gives rise to a strong ferromagnetic Zener double exchange interaction.[46] On the other hand, in n-type materials the electrons in the conduction band move essentially in the Zn 4s orbitals and all the cobalt ions are in the divalent state with the consequence that there is no double exchange interaction.[1] In this later case corresponding to ZnO-based DMS, the RKKY magnetic interaction[47] mediated by free carriers has been advanced as a potential source of ferromagnetism. However, this interaction does not play any role, because a ferromagnetic arrangement of the Co^{2+} magnetic moments would lead to a net magnetization at saturation per Co comparable to 2 μ_BS, with $S = 3/2$ the spin of Co^{2+} ions. This is more than 1 order of magnitude larger than the moment experimentally observed (0.12 μ_B) in this work and in prior works as well.

In a different approach, a ferromagnetic exchange mechanism involving oxygen vacancies V_O, which are double donors, was recently proposed in magnetically diluted tin oxide based semiconductors[16] (yet it remains to be demonstrated that the ferromagnetism is intrinsic in this material). In such oxides the overlap of the F-center electron orbitals with the d orbitals of the neighboring paramagnetic spins (TM) to form TM−V_O−TM groups is crucial for the proposed ferromagnetic coupling. But again, the possibility that such an effect drives a homogeneous cooperative ferromagnetic ordering of the ZnO-based DMS is ruled out by the fact that the magnetization at saturation, when it exists, is much too small. The F-centers, and actually any donor, can, however, generate inhomogeneous ferromagnetism by forming bound magnetic polarons. Indeed, such magnetic polarons are able to spin-polarize the Co^{2+} ions inside the polaron orbital, so that they act as macrospins giving rise to a magnetic moment that saturates easily under the application of an external magnetic field. Such a polaron effect has also been observed in $Zn_{1-x}Mn_xO$.[4] However, polaron effects are best observed at smaller transition metal concentration, because important antiferromagnetic (AF) superexchange interactions tend to oppose the formation of the bound magnetic polarons at larger concentrations x, where the probability of finding nearest neighboring AF pairs increases.[4]

Even though the synthesis process allowed us to synthesize $Zn_{0.84}Co_{0.16}O$ free from secondary phases, the EPR and magnetization measurements have shown that under moderate heating at 400 °C it is decomposed into $Zn_{0.92}Co_{0.08}O$ particles and Coclusters. The well-crystallized $Zn_{0.92}Co_{0.08}O$ part is confirmed by the X-ray analysis and the reduced composition is confirmed by the Curie−Weiss behavior of the intrinsic part of the magnetic susceptibility. The Co-cluster part could not be evidenced by the X-ray analysis because the size of the particles is too small and/or the Co-clusters are not well crystallized. To confirm the nature of the magnetic clustering, we have heated samples at the same temperature 400 °C, but for longer times (up to 12 h), so that the Co-clusters might increase in size. The X-ray analysis of such samples reveals the presence of hcp Co clusters crystallized in the compact hexagonal structure. The temperature of 400 °C is thus sufficient to crystallize Co clusters in its most stable form. This result confirms that the Co-clusters in sample B have not been detected by X-ray analysis because of their small size. Note that the choose of a heating temperature of 400 °C in the present study, was motivated by the TGA and temperature resolved spectroscopy analyses, which show that between 300 and 400 °C, important surface modifications take place in sample A, and suggest eventual magnetic properties variation between the as-produced powder and the subsequently heated one at 400 °C.

Let us now discuss the physicochemical process that is responsible for the precipitation of Co under the form of Co clusters at the origin of the ferromagnetic component. This phenomenon is related to the surface modification. Indeed, the structural analysis indicates a significant decrease in the oxygen content after heating. Unfortunately a quantitative analysis of the oxygen deficiency is not possible. Nevertheless, the IR study has shown that the as-produced particles are oxygen-capped through the absorption of diethyleneglycol and acetate species, whereas the heated ones (sample B) are almost free from adsorbed organic molecules. Moreover, the TG coupled with mass analysis has shown that the organic species, diethyleneglycol for instance, depart from the surface of the particles at a temperature higher than their boiling point, involving their decomposition, which is rather characteristic of chemisorbed species. We can thus speculate that desorption of these molecules generates surface oxygen vacancies. Now if these vacancies stay at the surface, they cannot explain the magnetic moment at saturation that is observed for sample B, because the surface to volume ratio for particles as big as 400 nm is orders of magnitude smaller than the ratio 0.12/5.1 of the magnetic moments abovementioned. The picture of oxygen vacancies that stay in the vicinity of the surface is then ruled out. Actually, we have to recall that the formation of Co-clusters is at the expense of Zn substituted Co, since the concentration x in $Zn_{1-x}Co_xO$ has been divided by a factor two during the heating process. It means that not only oxygen but also the cobalt must have diffused. The fact that the diffusion of these elements has

(45) Risbud, A. S.; Spaldin, N. A.; Chen, Z. Q.; Stemmer, S.; Seshadri, R. *Phys. Rev. B* **2003**, *68*, 205202.
(46) Zener, C. *Phys. Rev. B* **1951**, *82*, 403.
(47) Ruderman, A.; Kittel, C. *Phys. Rev. B* **1954**, *96*, 99. (b) Kasuya, T. *Prog. Theor. Phys.* **1956**, *16*, 45. (c) Yoshida, K. *Phys. Rev. B* **1957**, *106*, 893.

been important is evidenced by the TEM experiments and the XRD analysis that have shown a modification of the shape of the particles, those of sample B being much more spherical. The fact that the wurtzite crystal structure is maintained in the diffusion process requires that the motions of cobalt and oxygen ions must be correlated. Actually, since the Coulomb attraction between Co^{2+} and O^{2-} is strong, we can envision a diffusion process of Co−O pairs from the bulk of the particles to the surface. This process can be quantified by noting that the Zn ions must remain in the cationic sites of the wurtzite lattice, so that the amount of products before and after the heating process must be equilibrated as follows

$$Zn_{0.84}Co_{0.16}O \rightarrow \frac{0.84}{0.92}Zn_{0.92}Co_{0.08}O + \left(0.16 - \frac{0.84}{0.92}0.08\right)Co + \left(1 - \frac{0.84}{0.92}\right)O \quad (9)$$

The two expressions inside the parentheses are equal, which amounts to the migration of Co−O pairs out of the particles. This expression can also be written

$$Zn_{0.84}Co_{0.16}O \rightarrow 0.91[Zn_{0.92}Co_{0.08}O] + 0.087Co + 0.0435O_2 \quad (10)$$

which emphasizes that the 0.087 Co are the Co clusters formed at the surface, whereas the oxygen gas (O_2) part has volatilized.

Another secondary phase that might have been formed during the heat treatment is CoO. However, CoO cannot be the source of ferromagnetism, because of the antiferromagnetic nature of the magnetic exchange interactions in this oxide. Actually, even if some authors report superparamagnetic behavior at high temperatures with remanant magnetization at low temperature because of the existence of uncompensated moments on the surface of these nanoparticles,[48] such a ferromagnetic contribution remains very weak, because it corresponds to a low-temperature (6 K) magnetization that does not exceed 0.05 μ_B/Co at $H = 20$ kOe. This value is clearly lower than that measured in our powder (sample B). We are then left with the model of metallic Co clusters, also sustained by our analysis of the EPR spectra. Indeed, the direct X-ray detection of Co clusters for longer annealing times at the same temperature of 400 °C allows us, by extrapolation, to identify the magnetic clusters as Co-clusters. In addition, CoO is very unlikely formed here, because the samples have not be placed in an oxidizing atmosphere during the heating at 400 °C. Indeed, we have checked that the particles do not exhibit any FM behavior when heated in an oxidizing atmosphere up to 400 °C, which gives evidence that CoO rather than Co clusters are formed in this case.

From our results, we can conclude that the liberation of oxygen evidenced by thermogravimetric measurements is accompanied with the formation of cobalt nanoparticles at the surface as a result of a correlated diffusion of Co and O species in the powder. Such a correlated motion can also been evidenced by the fact that the heating at 400 °C did not introduce a significant n-type conductivity. Let us recall that isolated oxygen vacancies are double donors. However, the absence of the associated infrared absorption in the 2 to 3 μm range according to the Drude's law proves that no significant carrier concentration has been generated in sample B. In any case, the results of our study show that the free carrier concentration is small and does not play any role in the magnetic behavior of the annealed samples.

A magnetic clustering effect similar to the one we have observed here has been evidenced in other magnetic semiconductors such as $LiFePO_4$ for instance. In that case, the $LiFePO_4$ particles have a size comparable to that of the $Zn_{1-x}Co_xO$ particles in the present work, and heating in neutral atmosphere at high temperature has also dramatic effects on the magnetic properties: Fe atoms also forms magnetic nanoparticles (of Fe_2P and Fe_2O_3) giving rise to superparamagnetism.[49] The same phenomenon is responsible for the ferromagnetic component in sample B, the nanosized clusters located at the grain boundaries (interface of crystallites), or the surface being now metallic cobalt clusters.

Conclusion

According to XRD, TEM, and optical absorption spectroscopy analyses, the as-produced and heated cobalt substituted ZnO powders appear to be homogeneous, single-phase materials, where cobalt is only detected as Zn substituted Co^{2+} in ZnO. The as-produced sample is paramagnetic without any ferromagnetic component in the magnetization curve. The ferromagnetic component is generated by heating the particles to only 400 °C for 1 h in a nonoxidizing atmosphere. It is due to the formation of Co clusters. The combined analysis of magnetic, EPR, optical, and thermal gravimetric experiments reveal that this Co cluster formation is due to a correlated diffusion of Co and O species, part of the oxygen being desorbed from the surface desorption, whereas the Co precipitates at the surface.

The present work shows that the control of the surface during the synthesis and subsequent treatments is essential. This conclusion is not specific to the mode of synthesis we have chosen, because heat treatments also change the properties of transition metal doped ZnO nanocrystals prepared by wet-chemistry route.[32] This process could well be at the origin of the different and contradictory results reported in the literature. Note also that this phenomenon is also not specific to the case of Co in ZnO, but can also be expected to occur for other transition metal elements in ZnO. It was argued in prior works[4] that Mn doped ZnO is a classical semimagnetic semiconductor with antiferromagnetic nn superexchange interactions. We find here that the same is true for Co doped ZnO. Actually, the extensive investigation of iron-based magnetic semiconductors, such as $LiFePO_4$[49] because of its interest as a cathode element of lithium batteries, has shown us that unless the synthesis is performed in presence of hydrogen as a reducing agent, extrinsic ferromagnetism is always observed, because of the formation of maghemite nanoclusters. It can easily be seen that the

(48) Zhang, H. T.; Chen, X. H. *Nanotechnology* **2005**, *16*, 2288.

(49) Julien, C. M.; Mauger, A.; Ait-Salah, A.; Massot, M.; Gendron, F.; Zaghib, K. *Ionics* **2007**, *13*, 395.

magnitude of the ferromagnetic component in Fe:ZnO, when it has been observed, also corresponds to the formation of these clusters. In that case, many authors have considered it as an intrinsic property of a new ferromagnetic semiconductor. Unfortunately, we have to face reality: 3d-transition-metal-doped n-type ZnO is not a ferromagnetic semiconductor with long-range order, contrary to prior claims. Magnetic measurements are sufficient to draw this conclusion. However to establish unambiguously the formation of hcp Co clusters and to determine their average size, because XRD and TEM experiments cannot reveal them, extended X-ray absorption fine structure spectroscopy (EXAFS) experiments are in progress at the Co K-edge on samples A and B.

Acknowledgment. The authors are indebted to J-Y. Piquemal, P. Beaunier, Y. Li, and A. Zarouk for their technical assistance.

CM802605U